

Retrieval of Forest Fire History in Far East Asia by Remote Sensing and Its Analysis with Biomass Burning Simulation and Climate Anomalies

Jan KUÇERA and Yoshifumi YASUOKA

*Institute of Industrial Sciences, The University of Tokyo,
4-6-1 Komaba, Meguro-ku, Tokyo 153-8505, Japan*

Abstract. This paper describes the creation of a forest fire history database for part of the Far East region of Asia using remotely sensed data, Advanced Very High Resolution Radiometer (AVHRR). The algorithm for burnt scar mapping utilizes an active fire detection technique together with detection of abrupt vegetation damage depicted by time series of the Normalized Difference Vegetation Index (NDVI). The forest fire database is stored in Geographic Information System (GIS) format, which permits easy utilization for further research. We used the forest fire database for three purposes: a) for simulating biomass burning, b) for estimating biophysical variables, and c) for correlating weather anomalies with the fire's occurrence.

Keywords: forest fires, AVHRR, database, biomass burning, LAI, FAPAR, NPP, weather records

1. INTRODUCTION

A knowledge of forest fire occurrence, extent and damage intensity is recognized as indispensable for forest and fire management as well as for ecological science. In order to predict changes in fire regimes in future global environmental change, historical fire patterns should be studied. The availability of fire data differs from region to region. Developed countries in Europe, US and Canada maintain high-quality fire records which are used for a variety of research. On the other hand, fire data from the other parts of the world are not available and long-term fire behavior is not monitored. In this case, remote sensing data archives can play a crucial role in the extraction of forest fire data during last nearly 20 years, if suitable remotely sensed data are available.

In this study we used the AVHRR data archive available at the Institute of Industrial Science of the University of Tokyo as our main data source for creating a forest fire database for the Far East region of Asia. High temporal resolution, acceptable spatial resolution, spectral bands suitable for burnt scar mapping and easy data access are the main reasons for selecting AVHRR as a main data source. The feasibility of this choice is backed by a vast amount of research utilizing AVHRR in forest fire monitoring and mapping (Cahoon *et al.*, 1994; Chuvieco

and Martín, 1994a, b; Flasse and Ceccato, 1996; Dwyer *et al.*, 1998; Kasischke *et al.*, 1999; Pereira, 1999; Fraser *et al.*, 2000; Li *et al.*, 2000a, b; Cuomo *et al.*, 2001). A sophisticated burnt scar mapping algorithm was designed and forest fire database was created. The GIS environment greatly enhanced database utilization.

The estimation of biomass burned during a fire event plays an important role in forest related research and management. We coupled the fire database with a terrestrial ecosystem model to estimate consumed biomass in a larch forest ecosystem.

The further utilization of the database and remotely sensed data involves the estimation of biophysical variables (leaf area index—LAI, fraction of absorbed photosynthetically active radiation—FAPAR and annual aboveground net primary production—ANPP) for vegetation affected by fire. So far, the estimation of such variables from remotely sensed data was done for undisturbed ecosystems (Running and Nemani, 1988; Myneni and Williams, 1994; Veroustraete *et al.*, 1996) and this study complements that research with new findings on disturbed vegetation.

The last part of the paper introduces the utilization of the forest fire database to analyze the relationship between fire occurrence and climatic anomalies. The spatial distribution of annual burned area is compiled against an isoline map of annual anomalies of temperature and precipitation and the result is analyzed graphically to show a clear dependency of burned area on climatic conditions.

2. CREATION OF FOREST FIRE DATABASE

2.1. Data description

The main satellite data source used in this work is the AVHRR on-board the NOAA satellite series. All the data were received at the Institute of Industrial Science, University of Tokyo, located in Tokyo, Japan. The raw data, which begin in 1983, are received and archived in 10-bit High Resolution Picture Transmission (HRPT) format. Daily afternoon passes (approximately from 12.30–16.00 PM) of NOAA-7, -9, -11 and -14 from 1984 to 2001 were utilized. Only the fire and vegetation season (from March to October) images were selected for processing. Winter scenes (from November to February) were not used, since there is no or very low vegetation and fire activity. The second reason for skipping winter scenes lies in the fact that the precision of reflectance measurement is reduced in winter months due to the low solar zenith angle (Cracknell, 1997). Typical NOAA scene coverage and the study region are shown in Fig. 1.

2.2 Data preprocessing

The raw AVHRR radiance data were processed with the Package for NOAA Data Analysis (PaNDA) software. The package includes format conversion, radiometric correction, atmospheric correction and geometric correction of HRPT data. A format conversion subroutine converts 10 bit data to 16 bit data. A radiometric correction process converts digital values to albedo in channels 1

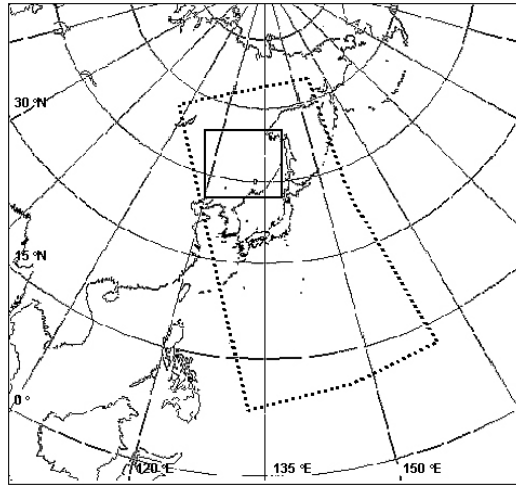


Fig. 1. NOAA scene coverage (dot line) and area of interest (solid line).

and 2, and to brightness temperature in channels 3, 4 and 5. Precise geometric correction is done in two steps. First, the approximate position and orientation of the image is determined from satellite orbital information. Secondly, the precise position and orientation is done by automatic matching to a set of Ground Control Points (GCPs), which were selected as part of the coastal lines. The reason for choosing GCPs on the coastal line rests on the easier discrimination of the boundary between cost and sea on thermal channel 4, which is used for matching. Details of PaNDA software can be found in PaNDA documentation (Shimoda *et al.*, 1998).

Since on 18-years time series of data were processed, it was necessary to take sensor degradation into account. The PaNDA software does not include such correction. The AVHRR sensors are not equipped with an on-board calibration target for visible and near infrared channels. The calibration of channel 1 and channel 2 for NOAA-7, -9, -11 and -14 was performed by a method using well-described ground targets, as explained by Rao and Chen (1999).

Before the processing, quicklook images provided with raw data were checked visually. Only scenes without apparent noise were selected for further processing. Raw data were radiometrically and geometrically corrected and transformed to the Plate-Caree (equirectangular) projection, resampled with a nearest neighborhood algorithm to 1.1×1.1 km pixel size and clipped to our area of interest. The precision of geometric correction is reflected in the value of overall transformation root mean square error (RMSE). Only scenes with RMSE smaller than 1 pixel were selected. In practically terms, the number of scenes per month was reduced from 30 or 31 to 20–25 due to apparent noise in raw data or poor geometric correction.

2.3 Description of mapping algorithm

The burned scar mapping algorithm consists of two parts. The first part is a multi-channel threshold algorithm developed for boreal environments. It detects hotspots during biomass burning provided the view is cloud-free. The algorithm has several limitations. It is prone to omission errors when the scene is cloudy or when smoke from the fire obscures the view. On the other hand, it misclassified as fire (commission error) such areas as water bodies (glint), bare soil and hot surfaces. The second part of the algorithm is based on the detection of abrupt lowering of NDVI in the time series. If there is an NDVI decrease (NDVI_d), that place is suspect for land cover change. The spots detected by this part of the algorithm are not only burned places but also clear cuts, and areas with vegetation stress during drought. The two parts are merged; if the pixel is marked as a fire by the multiple channel threshold hotspot algorithm and the NDVI has an appropriate decrease at the same time, the pixel is marked as a real burned pixel (RBP). RBP are pixels which were “seen” during a fire event. In order to involve pixels which surround RBP and were marked as NDVI_d but not as RBP (e.g. these pixels were covered by clouds but were actually burned and experienced NDVI decrease), the RBP are used as a base for extrapolating among NDVI_d pixels surrounding RBP in order to delineate a whole burned area.

The algorithm was applied only in the forest areas that were extracted from Eurasia Land Cover Characteristics Data Base (http://edcdaac.usgs.gov/glcc/euras_int.html). The vegetation map is derived from NOAA/AVHRR and thus the resolution well matches the data presented here.

2.3.1 Multi-channel threshold algorithm

The multi-channel threshold algorithm was adopted from Li *et al.* (2000a). The algorithm was designed for a boreal zone environment and for similar tree species in the Far East study area. The detailed physical explanation of the algorithm is described in Li *et al.* (2000a). The algorithm was applied to each NOAA scene in the study area, and the pixel that passed the test was marked as potential fire pixel (PFP). After fire detection processing, monthly PFP masks for period of 1984–2001 were compiled.

2.3.2 NDVI abrupt change detection algorithm

The NDVI 30-day composites were created before further processing. The maximum value compositing criterion was used, which preferably selects cloud free and close-nadir pixels (Goward *et al.*, 1994). The monthly (from March to October) NDVI composites for years 1984–2001 were available after compositing.

The algorithm for abrupt NDVI change is based on analyzing NDVI post-fire behavior on several burned areas. It was found that NDVI decrease, which occurs after a fire, persists only three or four years after fire event; thereafter the NDVI yearly pattern is almost the same as for an unburned area. The main reason for this NDVI behaviour is explained by vital shrub and herbaceous regrowth (Kasischke and French, 1997). An example of time series data with a severe fire event in 1987 is shown in Fig. 2, which shows a comparison between burned and adjacent unburned area of the same size and species distribution; NDVI values were

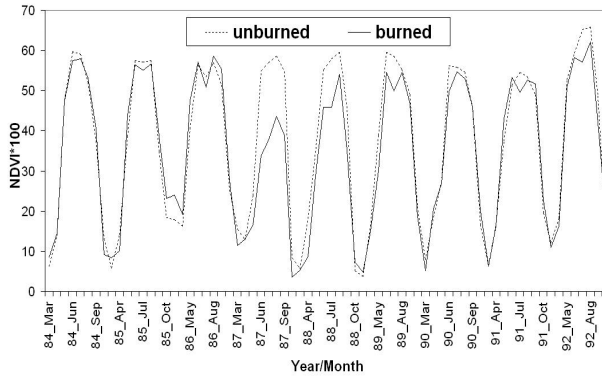


Fig. 2. Comparison of NDVI inter annual changes for unburned and burned and area.

averaged for each area. This burning occurred during the great China fire (Cahoon *et al.*, 1994). The property of regressing the NDVI pattern of the burned site was used to detect potential fire.

For each pixel, time series of each month for all 18 years were created: 18 NDVI values from the same month of all years make a time series set. As a result, each pixel has 8 time series sets of different 8 months. Each time series set was sorted with respect to value of NDVI (the smallest value first, highest last). The eight-year window was then moved along the 18 years sorted time series from beginning to the end (e.g. first position of the window contained first eight years of sorted NDVI set, second position of the window contained members from the second to the ninth year, etc.). For each position of the window the mean and standard deviation of NDVI were computed. The position with smallest standard deviation was selected as a base position. An eight-bin window was selected for two reasons. First, the 8 years among 18 years are supposed to represent "standard" values for normal vegetation condition, which differs only due to the random noise and natural vegetation growth and not due to substantial NDVI change. The second reason for selecting eight values is the assumption that eight members are a sufficient sample for computing the statistical characteristics of standard NDVI.

A new value of the smaller NDVI adjacent to the searching window was then examined to see whether or not it belongs to the same statistical sample as the basic eight search window values. A new value was accepted after passing the following statistical test (Bohm *et al.*, 1990):

A new mean was computed from nine values (e.g. eight basic values from searching window and new tested value).

The following characteristic was computed:

$$u_{(n)} = \frac{l_{(n)} - x_{(n)}}{\sigma_{(n-1)}} \quad (1)$$

where $u_{(n)}$ = tested characteristic, $l_{(n)}$ = tested value (in this case first lowest value left from searching window), $x_{(n)}$ = mean from all values (including new tested value), $\sigma_{(n-1)}$ = standard deviation computed from basic window, n = number of values in the sample.

If the tested characteristic was smaller than a critical value for the appropriate number of samples (n) listed in Bohm *et al.* (1990), the value $l_{(n)}$ was considered to be from the same statistical sample and no abrupt change was discovered. New $\sigma_{(n-1)}$ was computed for all nine values and those nine values were considered as the base sample for testing the next value.

If the nearest lower value of NDVI was not approved as an abrupt change, the closest higher value was tested with the same procedure to decide whether or not it belongs to the same statistical sample. The search window was thus expanded for smaller and higher values, step by step. If the tested value did not pass the test, it was marked as an abrupt change in NDVI.

Each pixel was examined using the test described above and suspicious pixels were marked. Abrupt change can appear at the lower or upper end of the sorted times series of NDVI. Lower abrupt change is caused by vegetation change and noise. As mentioned before, the vegetation change includes not only fire events but also clear cutting and other vegetation degradation. Upper abrupt change can be considered as noise in the data due to satellite degradation or unknown error in the raw data.

After processing 18 years' time series for each of eight months (March–October) and marking pixels with NDVI decrease (NDVId), total of 144 NDVId masks were created.

2.3.3 Combination of fire mask and NDVI decrease mask

The next step in processing was combining fire masks with PFP and NDVId masks. Both masks were first smoothed using a 3×3 mode filter. The PFP mask for each month was combined with NDVId masks for three subsequent months. Selection of subsequent months rather than “burning” month is based on the fact that fire could occur after the date that was selected as the maximum NDVI value in the compositing procedure and there would not be any abrupt NDVI change due to fire at all. Examining three subsequent months after each month ensures that fire really happened and has its signature at least in three subsequent months. This procedure confirms that fires which last longer and across the months are included. If the PFP in a given month was marked as a NDVId pixel in three subsequent months it is supposed to be real burned pixel (RBP) and is marked in the NDVI composite for each of three subsequent months.

As mentioned previously, RBP are pixels which were “visible” during a fire event. If the pixel which belonged to a burning patch was obscured by clouds or smoke from fire, it was not detected as PFP and subsequently as RBP but it was marked as a pixel with NDVI decrease (NDVId). In order to involve such pixels

Table 1. Annual burned areas in each region (km²).

Year	Amur	Khab.*	Prim.*	Heil.*	Jilin	Nei M.*	Total
1984	843.6	4578.0	45.2	298.8	16.0	66.8	5848.4
1985	451.5	878.1	158.2	632.3	102.9	44.7	2267.7
1986	4385.6	1973.2	236.6	1871.9	26.5	222.0	8715.8
1987	8082.2	2510.2	672.7	6703.2	23.8	204.4	18196.5
1988	520.5	4601.0	344.1	377.1	135.2	156.8	6134.6
1989	4173.3	844.5	219.5	433.0	59.7	31.7	5761.5
1990	764.4	405.9	75.3	217.5	4.8	79.5	1547.4
1991	356.9	809.2	209.8	715.0	17.5	53.8	2162.1
1992	4823.1	6023.4	1999.4	4957.2	686.9	2250.2	20740.2
1993	2385.8	2899.0	508.3	879.7	171.6	255.6	7100.2
1994	1390.1	1076.6	522.7	879.1	642.4	756.4	5267.2
1995	145.0	240.7	2.8	108.7	1.2	58.0	556.4
1996	15061.1	4206.3	98.2	1537.3	7.8	54.0	20964.8
1997	69.3	429.9	129.3	49.5	10.3	1.1	689.4
1998	2722.6	17821.4	398.9	516.2	16.7	34.1	21509.9
1999	1170.3	2157.1	378.2	773.7	0.0	74.4	4553.8
2000	9520.3	2133.5	4182.1	22333.2	8794.1	5165.1	52128.3
2001	8123.0	2099.2	797.9	16994.4	1495.8	3679.5	33189.8

in a burned patch, the simple region growing technique was employed in each of three subsequent monthly NDVI composites.

If the pixel was marked as NDVI_d but not as PFP, the simple 3×3 window surrounding the pixel was searched. If at least 3 RBP were not found in search window, the NDVI_d pixel was not marked as RBP and decrease of NDVI was supposed to be caused by noise or other non-fire related vegetation change. If at least 3 RBP were found in the neighborhood of an examined NDVI_d pixel, the mean (M) and standard deviation (SD) of NDVI of these RBP were computed. If the NDVI value of the examined pixel lay within the range of $M \pm SD$, the pixel was marked as RBP.

This step was repeated fifty times in order to let the region grow sufficiently. The number of repetitions was based upon observation of real fire locations in 1998, where no burned patches exceeded a size of approximately 50 pixels in diameter (i.e. about 25 km in the middle latitude of the study area). Theoretically, if the continuous burned patch is bigger and only three pixels in the burned patch were marked as PFP, then the boundary zone of the burned patch would be missing. However, it would be a real exception, if the burned patch of such size was detected only by such a small number of PFP, therefore the number of repetitions (50 times) is supposed to be sufficient.

Using this procedure, the RBP mask was obtained for each month, finally being compiled to give the annual burned area product. Validation was performed with several known burned areas in Heilongjiang province, Khabarovsk region and with available Landsat data for fires in 1998. Agreement was found to be adequate. The burned area for each year and administrative region is shown in

Table 1. The internet version of the entire forest fire database is available at <http://simserv.e.iis.u-tokyo.ac.jp/publish/init.html>.

3. BURNED BIOMASS ESTIMATION

In order to estimate the amount of biomass consumed during the fire event, the terrestrial ecosystem model Sim-Cycle was employed (Ito and Oikawa, 2002). Sim-Cycle simulates carbon allocation during vegetation growth in each of five ecosystem compartments: leaf, stem, root, litter and mineral soil. The amount of allocated biomass depends on species compositions, soil and climatic conditions.

In this study we simulated the biomass development for the case of a larch stand that was affected by fire. The ecosystem was brought from its initial state (0.5 t C ha^{-1} in each compartment) to the stabilized state, when Net Ecosystem Production (NEP) was practically zero, i.e. the release and uptake of carbon were equal. The biomass allocated to each compartment was compared with values found in the literature. The average of carbon allocated to live phytomass (leaf, stem and root) was estimated to be 31.4 t C ha^{-1} , which is in agreement with 27.8 t C ha^{-1} , the value given by Alexeyev *et al.* (2000) for the Far East region.

After that, the biomass burning was introduced through reallocation of biomass. The fraction of biomass consumed by fire in each compartment was supposed to be 100% for leaf, 30% for stem and root and 25% for litter, which are characteristic of severe fire conditions (Shvidenko and Nilsson, 2000). The total amount burned was then computed to be 12.1 t C ha^{-1} , which is with 11.3 t C ha^{-1} given by Cahoon *et al.* (1994) and 10.8 t C ha^{-1} given by Shvidenko and Nilsson (2000). The rest of dead biomass was directly reallocated to the litter. The simulation of biomass regrowth was then performed and time series of LAI, FAPAR and ANPP were obtained.

4. ESTIMATION OF BIOPHYSICAL VARIABLES FOR BURNED AREA

Since the NDVI reflects the vegetation conditions, it can be used to estimate biophysical variables LAI, FAPAR and ANPP, which are usually measured by ground techniques. LAI is the total leaf area per square meter. Generally, the higher LAI, the higher NDVI that is expected. FAPAR is the ratio of absorbed photosynthetically active radiation (APAR) and incoming photosynthetically active radiation (PAR). Higher FAPAR values usually result in higher photosynthesis and therefore higher NDVI. ANPP is the amount of biomass accumulated in vegetation and a higher value should result in elevated value of NDVI. The meaning and justification for connecting vegetation index and other measures derived from satellite observation to biophysical variables can be found in Veroustraete *et al.* (1996), Tian *et al.* (2000), and Dong *et al.* (2003).

The NDVI time series created for the burnt scar mapping algorithm were connected to time series of LAI, FAPAR and ANPP simulated by Sim-CYCLE. Pairs of time series for burned and unburned areas in larch forest were used. Nonlinear regression was used to establish the equations. The first 18 years of

time series of LAI and FAPAR (both variables were rapidly increasing) were connected with the NDVI time series for burned site; the NDVI time series of unburned site was connected with stabilized LAI and FAPAR (stabilization was reached after 50 years from fire). Both equations were formed in monthly steps. The relationship between NDVI and ANPP was searched in annual cumulative manner (so the annual ANPP_A was obtained) as suggested by Goward and Dye (1987) and Running and Nemani (1988). The annual sum of the productivity and NDVI is justified by the fact that ANPP is accumulating during the year, so the annual sum of NDVI better reflects this phenomenon.

The relationships have the following form:

$$BV = a + b \cdot VI \cdot (1 - e^{-c \cdot t}) \quad (2)$$

where BV = biophysical variable (LAI, FAPAR or ANPP_A), a, b, c = coefficients, VI = monthly resp. annual NDVI for LAI, FAPAR resp. ANPP_A, t = time in months (LAI, FAPAR), in years (ANPP_A).

The values of coefficients, RMSE and correlation coefficient R for each BV are:

LAI: $a = 0.18$ (0.13), $b = 0.0923$ (0.006), $c = 0.005$ (0.001), $R^2 = 0.71$ ($n = 256$);
 FAPAR: $a = 0.2$ (0.02), $b = 0.015$ (0.0006), $c = 0.011$ (0.0012), $R^2 = 0.82$ ($n = 256$);

ANPP_A: $a = 0.23$ (0.3), $b = 0.016$ (0.0009), $c = 0.055$ (0.012), $R^2 = 0.94$ ($n = 32$).

It must be stressed that the equations are valid only for larch forest biome. This study considered, only larch forest since this species is major in the region. Further species remain for further investigation. All relationships are time-dependent. A few years after the fire, the rapid increase of biophysical variables reflects vegetation regrowth. After about 30 years, the time dependency is not significant and gradually disappear with longer time after the fire. Equations suggest that the fire disturbance must be taken into account when estimating biophysical variables from satellite data. The time from the fire event is an important factor influencing the NDVI value as well as biophysical variables.

5. FIRE OCCURRENCE AND CLIMATIC ANOMALIES

The created forest fire database was further used to investigate the relationship between fire occurrence and climatic anomalies. As principal data source of weather data, the Monthly Climatic Data for the World obtained from Japan Meteorological Agency (JMA) was used. The data contain monthly weather observations from approximately 1300 stations throughout the world. The following weather parameter are available: temperature, temperature anomaly, normalized temperature anomaly, precipitation, precipitation ratio, quintile, the number of days which precipitation was more than 1 mm, vapour pressure, sunshine duration, sunshine duration ratio, observed pressure, sea level pressure.

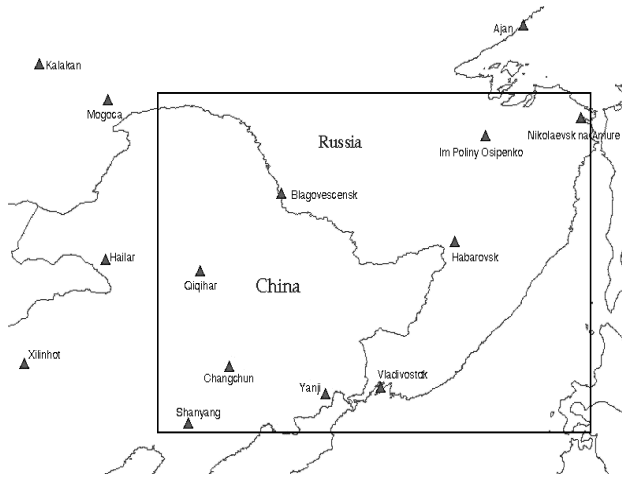


Fig. 3. Spatial extent of study area and forest fire database (rectangle) and location of observation stations used (triangles).

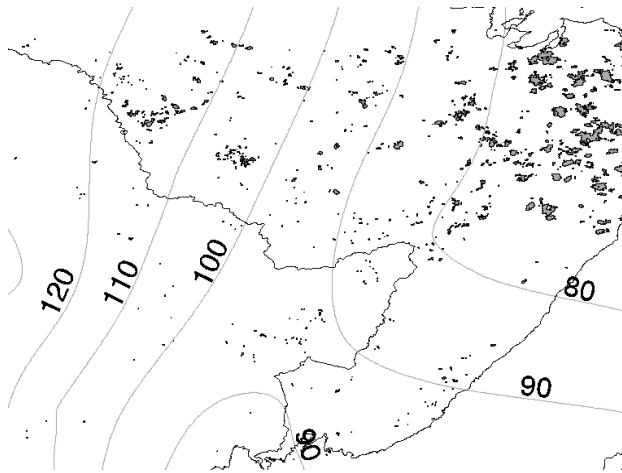


Fig. 4. Annual rain anomaly (in %) isolines for year 1998 overlaid with forest fire polygons.

This study utilized only observations from 14 stations located in the area of interest. The station spatial distribution can be seen in Fig. 3. The records used for the relationship with forest fire occurrence consist of temperature anomaly and precipitation ratio. These parameters are considered to have the closest connection with fire regime, compared to the others. Temperature anomaly shows the difference in degree Celsius between actual monthly temperature mean and long-term average temperature for a given month. The higher the value is, the

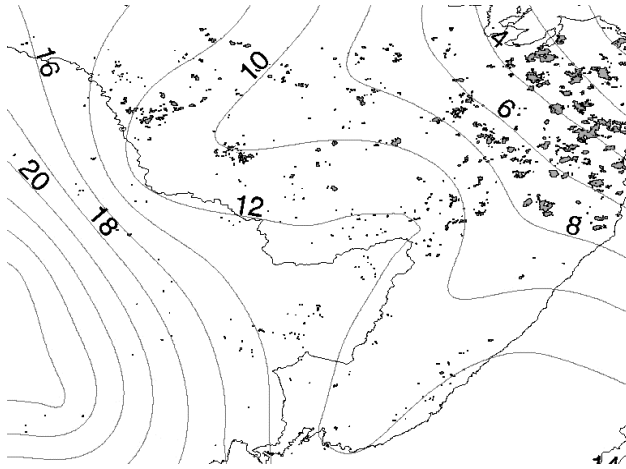


Fig. 5. Annual temperature anomaly (in °C) isolines for year 1998 overlaid with forest fire polygons.

warmer the weather was. The precipitation ratio expresses the percentage of actual monthly precipitation mean and long-term mean for a given month. A value below 100% means a drier month, above 100% is a wetter month. If the data for a certain month were not available (due to the station malfunction, repair or data loss), the long-term averages were taken as observed values.

In order to compare the monthly weather anomalies with annual burned areas, the annual temperature anomaly and annual precipitation anomaly were introduced. The annual temperature anomaly is the sum of monthly temperature anomalies. If the sum is higher than 0, the year is supposed to be warmer than the long term average; a negative value means a colder year. The annual precipitation anomaly is the average of monthly precipitation ratios. If the value is higher than 100%, the year is considered to be rainier; a value smaller than 100% means a drier year.

The data from stations were used as a base for interpolation and yearly isoline maps of annual temperature precipitation anomalies were created. (Example of year 1998 is shown in Figs. 4 and 5, respectively.) These maps were then overlaid with the maps of forest fire polygons for each year from 1984 to 2001. If the pixel was affected by fire, its temperature and precipitation anomalies were recorded. The number of pixels with the same temperature and precipitation anomaly is plotted on a color scale in Fig. 6.

As can be seen from Fig. 6, most of the forest fire occurred when the precipitation anomaly takes values from 65% to 95% of the long term mean. The relevant interval of temperature anomaly ranges from 3°C to 9°C above average. However, some fire occurrence was recorded outside of these ranges, especially in the range of -12°C to -15°C for annual temperature anomaly, which means the at fire occurrence depends more on water shortage than on temperature. It must

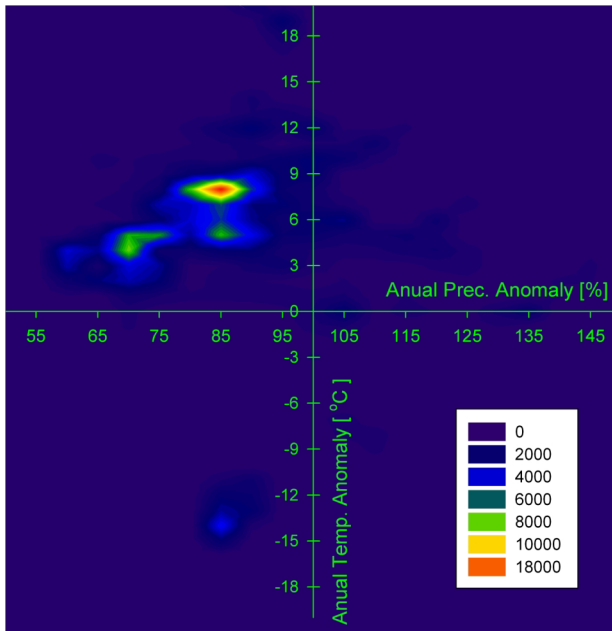


Fig. 6. Number of burned pixels (expressed as color scale) against annual precipitation and temperature anomalies. Drier and warmer years have values less than 100% for precipitation and greater than 0 for temperature anomaly.

be noted that annual anomalies also include data from winter months, e.g. outside of the fire season. Even though winter monthly anomalies do not have a direct influence on fire occurrence, they can have an indirect influence on the water regime of a given location and on water availability during the fire season, so they were also included in the analysis.

Even though the annual temperature and precipitation anomalies are rather rough weather indices, they clearly show fire dependence on temperature and water availability.

6. CONCLUSIONS

In this paper we have described the technique for creating a forest fire database for boreal forest in Far East Asia. If the appropriate amount of data is available, the algorithm can be used in other boreal regions for long-term burned scar mapping.

We have also outlined several potential uses of such a fire database. Important results were obtained justify the usefulness of forest fire database and encourages further research. The internet version of the database helps to share fire information with the broader community of researchers from various scientific fields, so further utilization can be expected.

REFERENCES

- Alexeyev, V. A., Birdsey, R. A., Stakanov, V. D., and Korotkov, I. A., 2000, Carbon Storage in the Asian Boreal Forests of Russia. In *Fire, Climate Change, and Carbon Cycling in the Boreal Forest*, edited by Kasischke, E. S. and Stocks, B. J., Springer-Verlag, New York, 239–257.
- Bohm, J., Radouch, V., and Hampacher, M., 1990, *Theory of errors and adjustment computation*. Geodetick_ a kartografick_ podnik, Praha (in Czech).
- Cahoon, D. R., Jr., Stocks, B. J., Levin, J. S., Cofer, W. R., III, and Pierson, J. M., 1994, Satellite analysis of the severe 1987 forest fires in northern China and southeastern Siberia. *J. Geophys. Res.* **99**(D9): 18,627–18,638.
- Chuvieco, E. and Martín, M. P., 1994a, Global fire mapping and fire danger estimation using AVHRR images. *Photogramm. Eng. and Remote Sens.* **60**(5): 563–570.
- Chuvieco, E. and Martín, M. P., 1994b, A simple method for fire growth monitoring using AVHRR channel 3 data. *Int. J. Remote Sens.* **15**: 3141–3146.
- Cracknell, A. P., 1997, *The advanced very high resolution radiometer*. Taylor and Francis, ISBN 0-7484-0209-8.
- Cuomo, V., Lasaponara, R., and Tramutoli, V., 2001, Evaluation of a new satellite-based method for forest fire detection. *Int. J. Remote Sens.* **22**(9): 1799–1829.
- Dong, J., Kaufmann, R. K., Myneni, R. B., Tucker, C. J., Kauppi, P. E., Liski, J., Buermann W., Alexeyev, V., and Hughes, M. K., 2003, Remote sensing estimates of boreal and temperate forest woody biomass: carbon pools, sources, and sinks. *Remote Sens. Environ.* **84**: 393–410.
- Dwyer, E., Gregoire, J. M., and Malingreau, J. P., 1998, A global analysis of vegetation fires using satellite images: spatial and temporal dynamics. *Ambio.* **27**(3): 175–181.
- Flasse, S. P. and Ceccato, P., 1996, A contextual algorithm for AVHRR fire detection. *Int. J. Remote Sens.* **17**(2): 419–424.
- Fraser, R. H., Li, Z., and Cihlar, J., 2000, Hotspot and NDVI differencing synergy (HANDS): a new technique for burned area mapping over boreal forest. *Remote Sens. Environ.* **74**: 362–376.
- Goward, S. N. and Dye, D. G., 1987, Evaluating North American net primary productivity with satellite observations. *Adv. Space. Res.* **7**(11): 165–174.
- Goward, S. N., Turner, S., Dye, D. G., and Liang, S., 1994, The University of Maryland improved global vegetation index product. *Int. J. Remote Sens.* **15**(17): 3365–3395.
- Ito, A. and Oikawa, T., 2002, A simulation model of the carbon cycle in land ecosystems (SIM-CYCLE): a description based on dry-matter production theory and plot-scale validation. *Ecological Modeling* **151**: 143–176.
- Kasischke, E. S. and French, N. H. F., 1997, Constraints on using AVHRR composite index imagery to study patterns of vegetation cover in boreal forests. *Int. J. Remote Sens.* **18**(11): 2403–2426.
- Kasischke, E. S., Bergen, K., Fennimore, R., Sotelo, F., Stephens, G., Janetos, A., and Shugard, H. H., 1999, Satellite imagery gives clear picture of Russia's boreal forest fires. *EOS* **80**(13): 141, 147.
- Li, Z., Nadon, S., and Cihlar, J., 2000a, Satellite-base detection of Canadian boreal forest fires: development and application of the algorithm. *Int. J. Remote. Sens.* **21**(16): 3057–3069.
- Li, Z., Nadon, S., Cihlar, J., and Stocks, B., 2000b, Satellite-based mapping of Canadian boreal forest fires: evaluation and comparison of algorithms. *Int. J. Remote Sens.* **21**(16): 3071–3082.
- Myneni, R. B. and Williams, D. L., 1994, On the relationship between FAPAR and NDVI. *Remote Sens. Environ.* **49**: 200–211.
- Pereira, M. C., 1999, A comparative evaluation of NOAA/AVHRR vegetation indexes for burned surface detection and mapping. *IEEE Trans. Geosci. Remote Sens.* **37**(1): 217–226.
- Rao, C. R. N. and Chen, J., 1999, Revised post-launch calibration of the visible and near-infrared channels of the Advanced Very High Resolution Radiometer (AVHRR) on the NOAA-14 spacecraft. *Int. J. Remote Sens.* **20**(18): 3485–3491.
- Running, S. W. and Nemani, R. R., 1988, Relating Seasonal Patterns of the AVHRR vegetation index to simulated photosynthesis and transpiration of forests in different climates. *Remote Sens. Environ.* **24**: 347–367.

- Shimoda, H., Fuke, K., Cho, K., Matsuoka, R., Hashimoto, T., Nemoto, T., Tokunaga, M., Tanba, S., and Takagi, M., 1998, Development of a software package for ADEOS and NOAA data analysis. *IEEE International Geoscience and Remote Sensing Symposium Proceedings Volume II*, pp. 674–676.
- Shvidenko, A. Z. and Nilsson, S., 2000, Fire and the carbon budget of Russian forests. In *Fire, Climate Change, and Carbon Cycling in the Boreal Forest*, edited by Kasischke, E. S. and Stocks, B. J., Springer-Verlag, New York, 298–311.
- Tian, Y. T., Zhang, Y., Knyazikhin, Y., Myneni, R. B., Glassy, J. M., Dedieu, G., and Running, S. W., 2000, Prototyping of MODIS LAI and FPAR algorithm with LASUR and LANDSAT data. *IEEE Trans. Geosci. Remote Sens.* **38**(5): 2387–2401.
- Veroustraete, F., Patyn, J., and Myneni, R. B., 1996, Estimating net ecosystem exchange of carbon using the normalized difference vegetation index and an ecosystem model. *Remote Sens. Environ.* **58**(1):115–130.

J. Kuçera (e-mail: kucera@iis.u-tokyo.ac.jp) and Y. Yasuoka (e-mail: yyasuoka@iis.u-tokyo.ac.jp)